Hindawi
Advances in Polymer Technology
Volume 2024, Article ID 4616496, 7 pages
https://doi.org/10.1155/2024/4616496

Research Article

Design, Fabrication, and Characterization of 3D-Printed Multiphase Scaffolds Based on Triply Periodic Minimal Surfaces

Josette Vigil[1], **Kailey Lewis**[1], **Nicholas Norris**[1], **Alp Karakoç**[2] and **Timothy A. Becker**[1,3]

[1]*Mechanical Engineering Department, Northern Arizona University, Flagstaff, AZ, USA*
[2]*Department of Communications and Networking, Aalto University, Espoo 00076, Finland*
[3]*Center for Materials Interfaces in Research and Applications, Northern Arizona University, Flagstaff, AZ, USA*

Correspondence should be addressed to Timothy A. Becker; tim.becker@nau.edu

Received 5 August 2022; Revised 9 November 2023; Accepted 18 November 2023; Published 4 January 2024

Academic Editor: Milan Mari

The present work investigates the influence of material phases and their volume fractions on the elastic behavior of triply periodic minimal surface (TPMS) scaffolds for the potential modeling of bone scaffolds. A graphical tool using TPMS functions, namely Schwarz-D (diamond), gyroid, and modified gyroid, was developed and used to design and additively manufacture 3D multiphase scaffold models. A PolyJet, UV-cured 3D-printer system was used to fabricate the various TPMS scaffold models using three polymer materials with high, medium, and low stiffness properties. All TPMS models had the same volume fractions of the three polymer materials. Final models were printed into cylinders with a diameter of 20 mm and a height of 8 mm for mechanical testing. The models were subjected to compressive and shear testing using a dynamic mechanical analysis rheometer. All samples were tested at physiologically relevant temperature (37°C) to provide detailed structural characterizations. Microscopic imaging of 3D-printed scaffold longitudinal and cross sections revealed that additive manufacturing adequately recreated the TPMS functions, which created anisotropic materials with variable structures in the longitudinal and transverse directions. Mechanical testing showed that all three TPMS 3D-printed scaffold types exhibited significantly different shear and compressive properties (verifying anisotropic properties) despite being constructed of the same volume fractions of the three UV-printed polymer materials. The gyroid and diamond scaffolds demonstrated complex moduli values that ranged from 1.2 to 1.8 times greater than the modified gyroid scaffolds in both shear and compression. Control scaffolds printed from 100% of each of the three polymers had statistically similar mechanical properties, verifying isotropic properties.

1. Introduction

Bone (osseous tissue) scaffolds act as supports for cell homing, colonization, and mechanical stability during bone tissue regeneration [1, 2]. They permit the transportation of nutrients, oxygen, and metabolic wastes as they are tailored to guide cellular growth and proliferation [3]. However, due to the complex structure of bone tissue porosity and interconnectivity for cellular and nutrient diffusion, the design and manufacturing processes of synthetic bone scaffolds are a challenge [4]. Triply periodic minimal surface (TPMS) functions may provide an option to simulate the complex interconnected scaffold structures of bone. TPMS functions have zero mean curvature and high surface-to-volume ratios, which may enhance the potential for future bone scaffold designs that have directional (anisotropic) mechanical properties that can promote cell proliferation, differentiation, and structural integrity [5–7]. TPMS scaffolds provide optimized correlation between the material phase fractions and stiffness while fulfilling functional grading, composition, and complex biological attributes [8, 9]. Investigations also show that TPMS functions may be suitable candidates (among beam-based structures, foams, lattices, etc.) for simulating bone scaffold composition by closely mimicking the complex cancellous and cortical layers [10–16].

Developments in additive manufacturing methods (e.g., UV-cured polymaterials, selective laser melting, selective laser sintering, stereolithography material jetting) and corresponding material technologies have accelerated the realization of complex scaffold geometries [17–19]. In recent years,

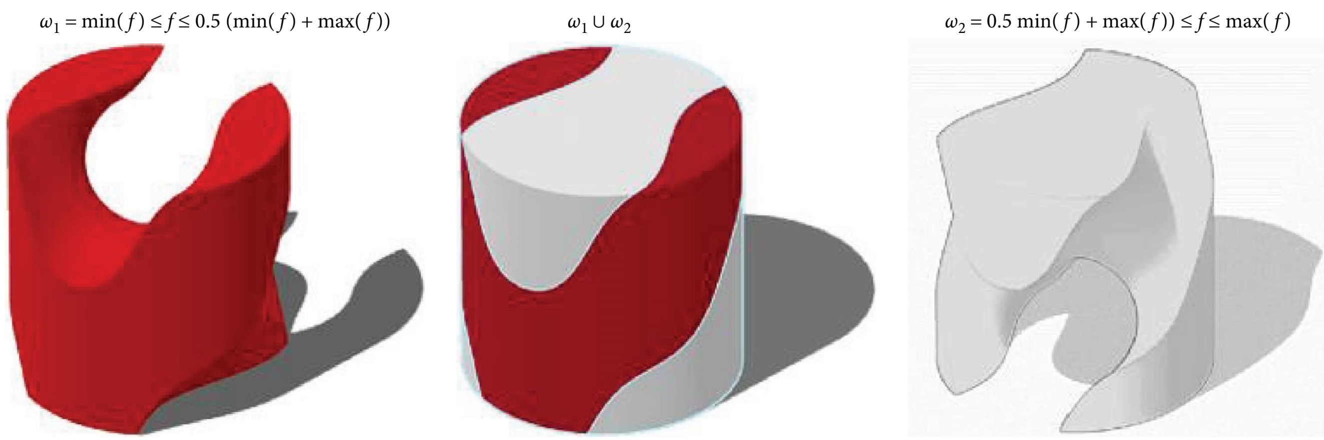

Figure 1: Schematic illustration of region-based multiphase TPMS scaffolds.

additively manufactured TPMS scaffolds have been widely investigated to explore their bionic performance. These investigations provide a foundation for the use of silicates and soluble colloids [20]. The ability to withstand intended mechanical loading without failure is a challenge in the design and manufacturing of TPMS scaffolds [21, 22].

This research assessed UV-cured, acrylate-based, 3D-printable polymers, identified as Vero® (stiff polymer) and Agilus® (soft polymer), as potential biomaterial candidates with controllable mechanical properties. This line of UV-cured, acrylic-based copolymers can be mixed at various proportions to make soft and flexible, medium stiffness, or hard and inflexible polymer sample types in the same print. The TPMS models were printed using an Objet260 Connex3 3D printing system (Stratasys, Eden Prairie, MN) to create intricate TPMS functions printed using the three polymer sample types. The 3D printability of macro and microstructural properties supports the control of various material stiffnesses and layering patterns based on the TPMS functions.

This study aims to test the potential biomimetic properties of TPMS functions additively manufactured to yield controllable anisotropic mechanical properties. Choosing three different layering patterns allowed for the quantification of the anisotropic material properties based on the TPMS function type.

TPMS function	TPMS scaffold (three phase regions)
Schwarz-D (diamond) $f(x, y, z) = \sin(x)\sin(y)\sin(z) + \sin(x)\cos(y)\cos(z) + \cos(x)\sin(y)\cos(z) + \cos(x)\cos(y)\sin(z)$	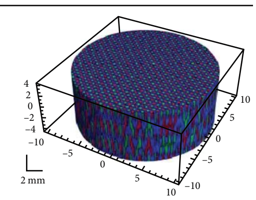
Gyroid $f(x, y, z) = \cos(x)\sin(y) + \sin(x)\cos(z) + \cos(y)\sin(z)$	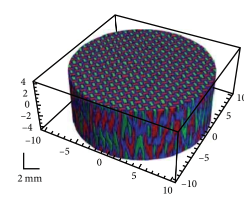
Modified gyroid $f(x, y, z) = \cos(x)\sin(y) + 2\sin(x)\cos(z) + 4\cos(y)\sin(z)$	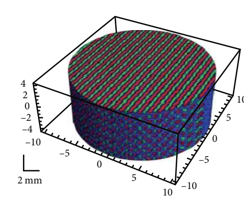

Figure 2: Surface functions $f(x, y, z)$ composing the TPMS scaffolds and their virtual depictions. The blue region represents the stiffer bone-like structures, while red and green regions represent softer tissue and cellular components, respectively.

2. Materials and Methods

2.1. Structure Design and Specimen Fabrication. 3D multiphase scaffolds were designed using a region-based approach with Schwarz-D (diamond) and two gyroid TPMS functions \hskip 6pt (Figures 1 and 2). Each TPMS scaffold was constructed with three phase regions at set volume fractions of 25%, 25%, and 50% with materials of soft, medium, and hard stiffness properties, respectively. The shear and compressive modulus of each material were also quantified. The resulting TPMS prints were also subjected to compressive and shear modulus testing at physiologically relevant temperatures (37°C). These tests were conducted on an HR-2 Hybrid DMA-Rheometer (TA Instruments, New Castle, DE), providing the complex (dynamic) modulus behavior consisting of storage and loss modulus data. Pure polymer prints were tested to quantify their isotropic mechanical behavior, compared to layered TPMS scaffolds using the same polymers but representing anisotropic mechanical properties [23]. In the structural design process, phase fractions and surface functions were used as input parameters for the region-based TPMS scaffold generation algorithm, available at https://github.com/metudust/Multiphase TPMSScaffold under an MIT license. Rather than adding thickness to the minimal surfaces, as is common practice

[24, 25], discrete regions $\omega_{i=1,2,\ldots,n}$ were defined with local minima $\min(f(x,y,z))$ and maxima $\max(f(x,y,z))$ of the investigated TPMS functions f (Equation (1)).

$$\omega_i = \alpha \cdot \max(f) + (1-\alpha)\cdot \min(f) \le f \le \beta \cdot \max(f) + (1-\beta)\cdot \min(f), \tag{1}$$

for which $0<\alpha\le 1$, $0<\beta\le 1$, $\alpha<\beta$, $\{\alpha,\beta\}\in\mathbb{R}$. The assembly of the discrete regions is shown in Figure 1.

Three phase regions and volume fractions were arranged into three TPMS functions based on literature confirming significant variation in the support structures oriented in the longitudinal and transverse directions. The three TPMS functions selected with highly variable structural orientations were diamond, gyroid, and modified gyroid [26–28]. The implemented functions and their graphical representations are listed in Figure 2. Red (25% volume fraction) and green regions (25% volume fraction) represent soft structures, such as connective tissue and cellular components, while blue regions (50% volume fraction) can represent stiff structures, such as cortical and cancellous bone. First, three samples of each of the three individual polymer materials were printed (100% volume fraction of each polymer material into 20 mm by 8 mm cylinders) to identify the mechanical properties of the individual print materials. The controls were mechanically tested for shear and compressive modulus with a dynamic mechanical analysis (DMA)-rheometer.

Next, three samples of each TPMS model (diamond, gyroid, and modified gyroid) models were printed (Figure 3). 3D printer resolution was 30 μm $\pm$10% for all samples. The 25% volume fraction of soft polymer (dark blue) was printed using pure Agilus-30®. The 25% volume fraction medium stiffness polymer (purple) was printed by mixing Agilus-30® and Vero Magenta®. The 50% volume fraction stiff polymer (light blue) was printed with pure Vero Cyan®.

After polishing the cylinder's cross-sectional (transverse) surface, sectioning the cylinders longitudinally, and imaging the cylinders at 5x magnification, the successful printing of the 3D-print TPMS patterns was verified (Figure 3).

2.2. Experimental Methods. Mechanical testing of the 3D-printed control and TPMS models was performed using nondestructive compressive and shear methods, $n = 3$ repeats. The mechanical testing determined the compressive and shear dynamic moduli across a physiologically relevant oscillatory frequency range (1–20 rad/s). All mechanical tests were performed on the DMA-rheometer with a quick-change Peltier plate, a 20 mm flat plate, and a solvent trap to maintain 37°C.

2.2.1. Compression Testing. Compressive loading of the control and TPMS models was based on physiological pressures ranging from 100 to 160 mmHg. These pressures were converted to Pascals and multiplied by the area of the flat plate and sample diameter (both 20 mm), yielding a force range of 4.19–6.70 N, respectively. The height of the scaffold at each preloaded force was noted. The axial displacement was set at 25% of the difference between these two heights, which was selected to mitigate excessive impact forces often seen from stiffer materials as the DMA-rheometer imposes dynamic compression levels at higher oscillation frequencies. To begin the test, the scaffolds were preloaded to 4.19 N. The flat plate dynamic compressive height was set, and the plate was oscillated across a frequency range of 1–20 rad/s and repeated three times on each scaffold sample (Figure 4(a)). The resulting data collected was the complex compressive modulus (E^*), which consists of elastic (storage) and loss (viscous) modulus data.

2.2.2. Shear Testing. To commence shear testing, the control and TPMS models were centered on the Peltier plate under the solvent-trap and preloaded to the same 4.19 N. An oscillatory shear strain of 1% was applied to each scaffold across the same frequency range of 1–20 rad/s and was repeated three times on each scaffold sample (Figure 4(b)). The resulting data collected was the complex shear modulus (G^*), which consists of elastic (storage) and loss (viscous) modulus data.

2.2.3. Statistical Analysis. All TPMS and control model tests were recorded with an average modulus and standard deviation. Using a statistical double-sided t-test, the gyroid, modified gyroid, and diamond TPMS prints were compared to each other and the three control models. The p values and % variance between each TPMS model and the control models were calculated. The results were considered statistically different if the p value was <0.05 (95% confidence).

3. Results

The control scaffolds exhibited shear and elastic moduli values that increased with the stiffness of each sample and the angular frequency. The diamond, gyroid, and modified gyroid TPMS prints, while containing the same volume fractions of control materials, each exhibited significantly different complex moduli in both the compressive and shear tests (Figures 5 and 6).

For statistical comparison of control and TPMS models, a physiologically relevant frequency of ~1 Hz (6 rad/s) was selected for further analysis of all scaffold properties. Storage, loss, and overall complex modulus for both compression (E^*) and shear (G^*) are reported (Table 1). Storage modulus represented >70% of the overall complex modulus in shear and >80% of the overall complex modulus in compression (exhibiting minimal loss modulus); therefore, all remaining figures were displayed with complex moduli results. Under compressive testing, the control scaffolds had E^* ranging from 1.37 to 8.88 MPa. The TPMS scaffolds E^* ranged from 3.62 to 5.48 MPa. The control scaffolds' percent standard deviation ranged from 7.8% to 8.6%, and the TPMS scaffolds' percent standard deviation ranged from 8.5% to 20.3% (Table 1).

As expected, all TPMS models had compressive moduli within the range of the stiff to soft polymer controls. All TPMS models were significantly different from each other

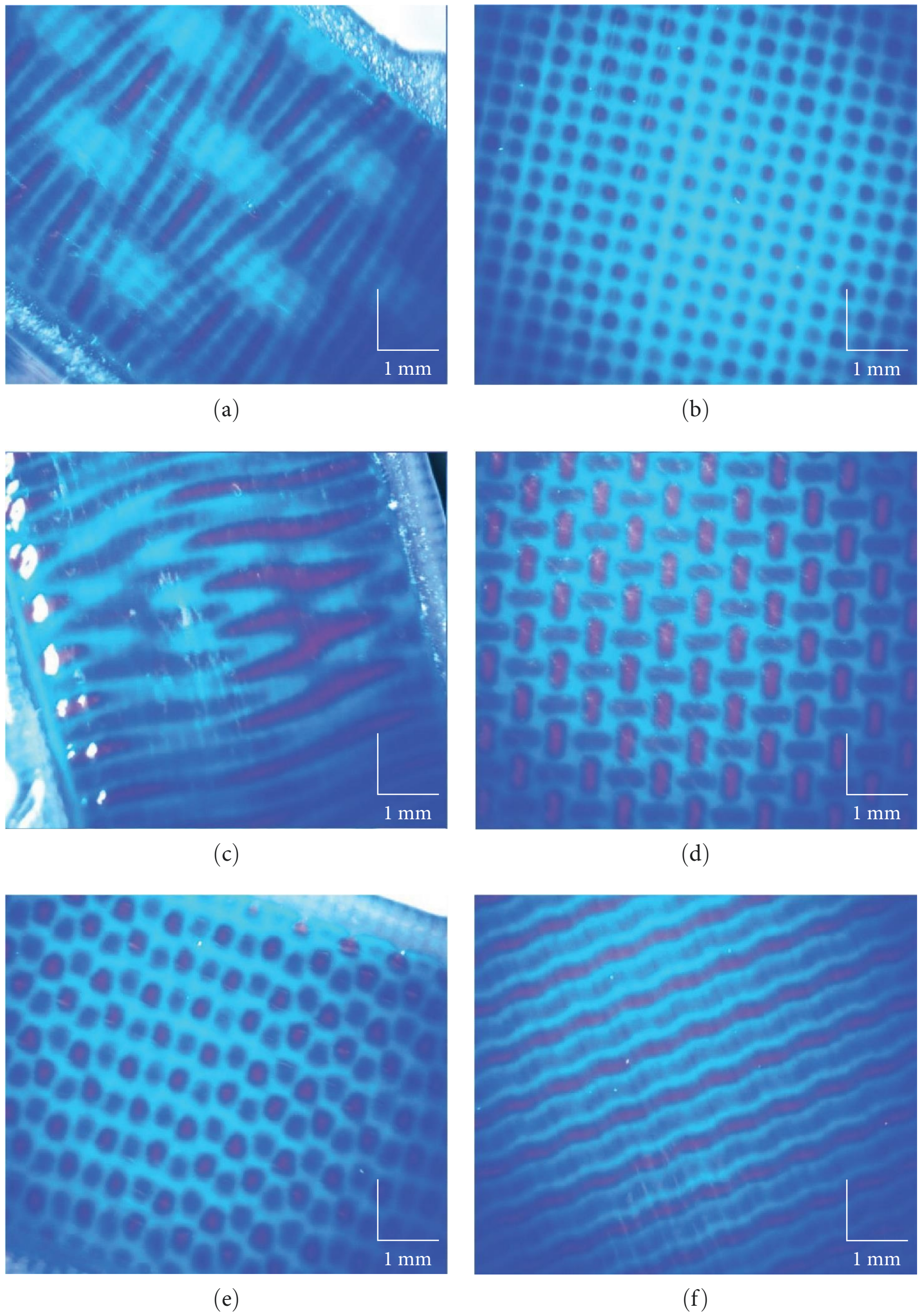

FIGURE 3: Images of the 20×8 mm 3D-print TPMS scaffolds, along with magnified images using an AmScope (Feasterville, PA) surgical microscope (5x): (a) diamond longitudinal-section; (b) diamond transverse-section; (c) gyroid longitudinal-section; (d) gyroid transverse-section; (e) modified gyroid longitudinal-section; (f) modified gyroid transverse-section.

(p value < 0.001, Figure 7), even though all models were printed with the same volume fractions of soft, medium, and hard polymer materials. The modified gyroid had the lowest compressive moduli at 87% of the gyroid compressive moduli and 57% of the diamond compressive moduli (E^*, p value < 0.001).

Under shear testing, the control scaffolds G^* ranged from .363 to 1.64 MPa. The TPMS scaffolds G^* ranged from 0.6 to 1.06 MPa (Table 1). The control scaffold percent standard deviation ranged from 4.2% to 7.2%, and the TPMS scaffold percent standard deviation ranged from 1.2% to 9.7%.

All TPMS models had shear moduli within the range of the stiff to soft polymer controls. All TPMS models were significantly different from each other (p value < 0.001, Figure 8). The modified gyroid had the lowest shear moduli, with 75% of the gyroid shear moduli and 56% of the diamond shear moduli (G^*, p value < 0.001).

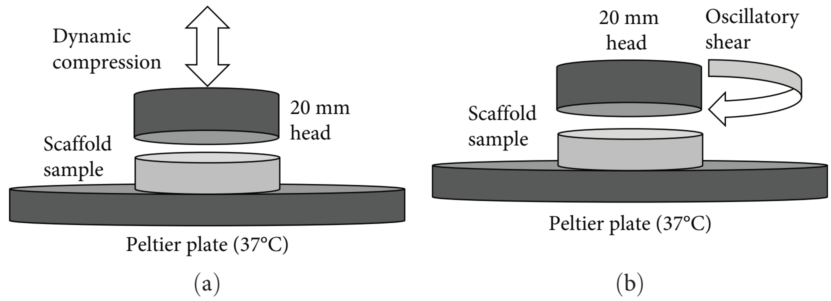

FIGURE 4: (a) Rheometer set up for dynamic compression testing; (b) rheometer set up for oscillatory shear testing.

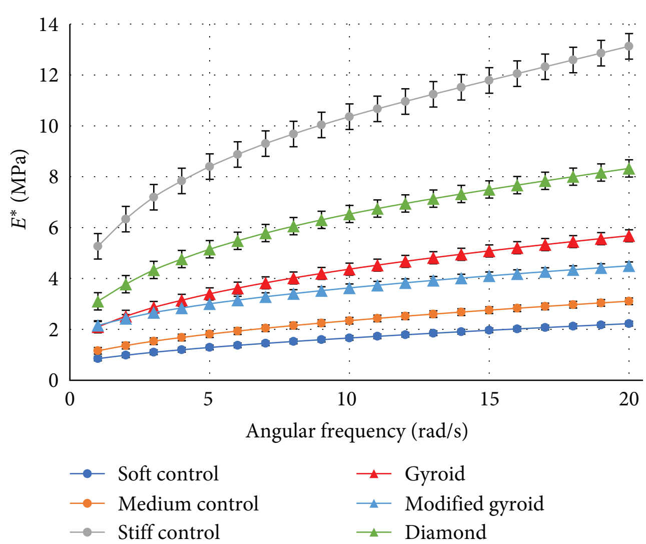

FIGURE 5: Compressive complex moduli (E^*) with respect to angular frequency for the control (soft, medium, stiff) and TPMS scaffolds (diamond, gyroid, and modified gyroid).

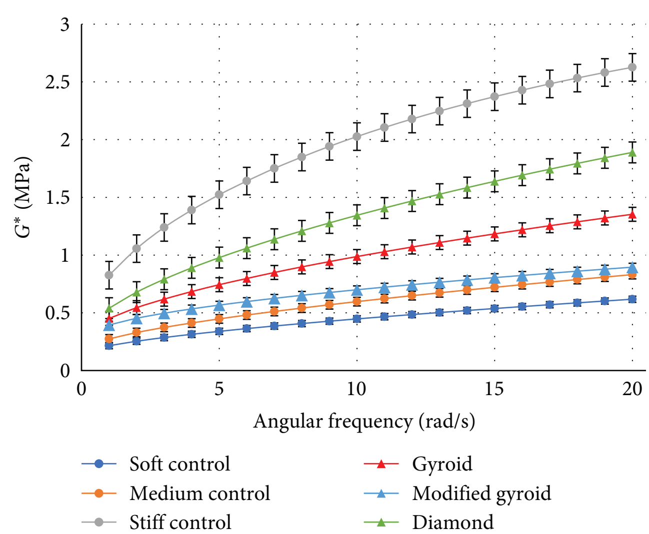

FIGURE 6: Shear complex moduli (G^*) with respect to angular frequency for the controls (soft, medium, stiff) and TPMS scaffolds (diamond, gyroid, and modified gyroid).

TABLE 1: Average mechanical data for controls and TPMS models.

	E^* (Mpa)	Error (%)	E storage (Mpa)	Error (%)	E loss (Mpa)	Error (%)	G^* (Mpa)	Error (%)	G storage (Mpa)	Error (%)	G loss (Mpa)	Error (%)
Soft control	1.37	7.8	1.15	6.84	0.79	22.4	0.36	4.5	0.29	3.63	0.21	6.17
Medium control	1.93	8.6	1.59	7.04	1.08	11.9	0.48	7.2	0.38	4.89	0.29	11.1
Stiff control	8.88	8.1	7.49	8.17	4.75	8.02	1.64	4.2	1.17	5.13	1.14	3.45
Gyroid	3.62	20.3	2.95	19.43	2.09	22.3	0.80	9.7	0.63	2.54	0.52	4.26
Modified gyroid	3.15	8.5	2.83	8.47	1.38	9.05	0.60	5.9	0.52	4.47	0.29	10.6
Diamond	5.48	15.7	4.39	15.86	3.28	15.7	1.06	1.2	0.78	1.48	0.72	1.04

Compression (E^*) and shear (G^*) complex, storage, and loss moduli for the control and TPMS models at 6 rad/s.

4. Discussion

As expected, the complex elastic and shear moduli for the investigated TPMS scaffolds exhibited properties within the moduli range of the control scaffolds. Variations in the complex moduli among the TPMS scaffolds confirmed that different layering patterns in the longitudinal and transverse directions yield adjustable anisotropic material properties. Each TPMS model had statistically different compressive and shear moduli from each other, even though each model was made with the same volume fraction of the three control polymer materials. The gyroid and modified gyroid models demonstrated lower complex moduli than the diamond model in both compression and shear. It is apparent, based on the mechanical behavior of the TPMS scaffolds, that the layering technique has a significant impact on material properties. TPMS functions can, therefore, be tailored to express variations in longitudinal and transverse properties, which lead to anisotropic model behavior. In future studies, we plan to mechanically test various TPMS models and compare

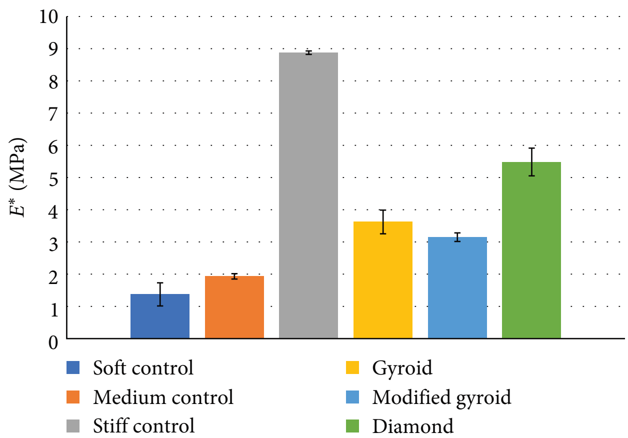

FIGURE 7: Compressive complex moduli (E^*) of the TPMS models and the control models at 6 rad/s.

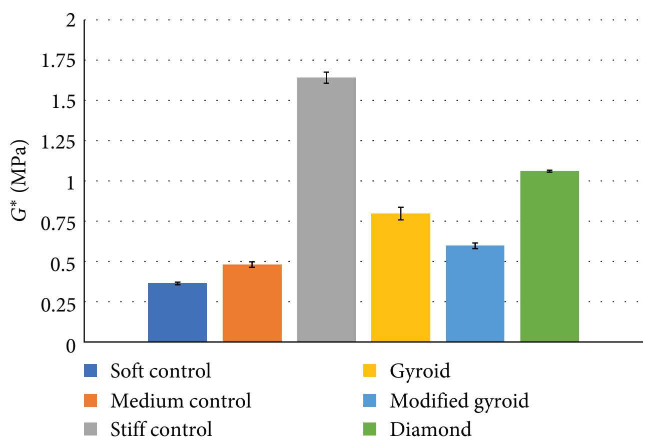

FIGURE 8: Shear complex moduli (G^*) of the TPMS models and the control models at 6 rad/s.

them to various natural extracellular matrix tissues and bone scaffolds (i.e., cortical and cancellous bony structures).

5. Conclusions

The printed TPMS equations had a considerable effect on the resulting anisotropic properties. The recorded complex moduli in both shear and compression for each sample were significantly different. The variance in material properties helped provide insight into the directional properties of each 3D-printed scaffold. The preliminary data gathered from the TPMS scaffolds indicate that variations in stiffness properties may be altered to potentially match the mechanical properties of bone or other tissues. Bones are inherently stronger in tension, compression, and bending than in shear. Developing implantable bone scaffolds that can closely approximate these variations with directional mechanical properties may dramatically improve bone regrowth, repair, and reorganization. Further investigations may lead to a new generation of scaffolds for bone tissue engineering that can be tailored to exhibit predictable material properties based on the measured compression and shear modulus values.

Data Availability

The corresponding author and the authors affiliated with Northern Arizona University can access the data. Data can be obtained by contacting the corresponding author (TAB).

Conflicts of Interest

The authors declare that they have no conflicts of interest.

Acknowledgments

AK gratefully acknowledges the Research Fellowship at the School of Electrical Engineering and funding from the Academy of Finland BESIMAL project (decision number 334197). TB acknowledges the resources of the Bioengineering Devices Laboratory at NAU and funding from the NIH (5R42NS097069-03).

References

[1] S. Bose, S. Vahabzadeh, and A. Bandyopadhyay, "Bone tissue engineering using 3D printing," *Materials Today*, vol. 16, no. 12, pp. 496–504, 2013.

[2] Ö. Keleş, E. H. Anderson, J. Huynh, J. Gelb, J. Freund, and A. Karakoç, "Stochastic fracture of additively manufactured porous composites," *Scientific Reports*, vol. 8, Article ID 15437, 2018.

[3] J. Santos, T. Pires, B. P. Gouveia, A. P. G. Castro, and P. R. Fernandes, "On the permeability of TPMS scaffolds," *Journal of the Mechanical Behavior of Biomedical Materials*, vol. 110, Article ID 103932, 2020.

[4] A. G. Mitsak, J. M. Kemppainen, M. T. Harris, and S. J. Hollister, "Effect of polycaprolactone scaffold permeability on bone regeneration *in vivo*," *Tissue Engineering Part A*, vol. 17, no. 13-14, pp. 1831–1839, 2011.

[5] S. Yu, J. Sun, and J. Bai, "Investigation of functionally graded TPMS structures fabricated by additive manufacturing," *Materials & Design*, vol. 182, Article ID 108021, 2019.

[6] L. Yang, C. Yan, C. Han, P. Chen, S. Yang, and Y. Shi, "Mechanical response of a triply periodic minimal surface cellular structures manufactured by selective laser melting," *International Journal of Mechanical Sciences*, vol. 148, pp. 149–157, 2018.

[7] C. Zhang, H. Zheng, L. Yang et al., "Mechanical responses of sheet-based gyroid-type triply periodic minimal surface lattice structures fabricated using selective laser melting," *Materials & Design*, vol. 214, Article ID 110407, 2022.

[8] A. P. G. Castro, T. Pires, J. E. Santos, B. P. Gouveia, and P. R. Fernandes, "Permeability versus design in TPMS scaffolds," *Materials*, vol. 12, no. 8, Article ID 1313, 2019.

[9] Y. Lu, W. Zhao, Z. Cui, H. Zhu, and C. Wu, "The anisotropic elastic behavior of the widely-used triply-periodic minimal surface based scaffolds," *Journal of the Mechanical Behavior of Biomedical Materials*, vol. 99, pp. 56–65, 2019.

[10] S. C. Kapfer, S. T. Hyde, K. Mecke, C. H. Arns, and G. E. Schröder-Turk, "Minimal surface scaffold designs for tissue engineering," *Biomaterials*, vol. 32, no. 29, pp. 6875–6882, 2011.

[11] D. Yoo, "New paradigms in internal architecture design and freeform fabrication of tissue engineering porous scaffolds," *Medical Engineering & Physics*, vol. 34, no. 6, pp. 762–776, 2012.

[12] D. Yoo, "New paradigms in hierarchical porous scaffold design for tissue engineering," *Materials Science and Engineering: C*, vol. 33, no. 3, pp. 1759–1772, 2013.
[13] A. Karakoç, K. Santaoja, and J. Freund, "Simulation experiments on the effective in-plane compliance of the honeycomb materials," *Composite Structures*, vol. 96, pp. 312–320, 2013.
[14] I. Christodoulou and P. J. Tan, "Crack initiation and fracture toughness of random Voronoi honeycombs," *Engineering Fracture Mechanics*, vol. 104, pp. 140–161, 2013.
[15] N. Yang and K. Zhou, "Effective method for multi-scale gradient porous scaffold design and fabrication," *Materials Science and Engineering: C*, vol. 43, pp. 502–505, 2014.
[16] N. Yang, L. Gao, and K. Zhou, "Simple method to generate and fabricate stochastic porous scaffolds," *Materials Science and Engineering: C*, vol. 56, pp. 444–450, 2015.
[17] H. Jinnai, H. Watashiba, T. Kajihara, Y. Nishikawa, M. Takahashi, and M. Ito, "Surface curvatures of trabecular bone microarchitecture," *Bone*, vol. 30, no. 1, pp. 191–194, 2002.
[18] A. Karakoç, V. K. Rastogi, T. Isoaho, B. Tardy, J. Paltakari, and O. J. Rojas, "Comparative screening of the structural and thermomechanical properties of FDM filaments comprising thermoplastics loaded with cellulose, carbon and glass fibers," *Materials*, vol. 13, no. 2, Article ID 422, 2020.
[19] Y. H. Zhang, X. M. Qiu, and D. N. Fang, "Mechanical properties of two novel planar lattice structures," *International Journal of Solids and Structures*, vol. 45, no. 13, pp. 3751–3768, 2008.
[20] J. Shi, L. Zhu, L. Li, Z. Li, J. Yang, and X. Wang, "A TPMS-based method for modeling porous scaffolds for bionic bone tissue engineering," *Scientific Reports*, vol. 8, Article ID 7395, 2018.
[21] C. Bonatti and D. Mohr, "Mechanical performance of additively-manufactured anisotropic and isotropic smooth shell-lattice materials: simulations & experiments," *Journal of the Mechanics and Physics of Solids*, vol. 122, pp. 1–26, 2019.
[22] N. Abbasi, S. Hamlet, R. M. Love, and N.-T. Nguyen, "Porous scaffolds for bone regeneration," *Journal of Science: Advanced Materials and Devices*, vol. 5, no. 1, pp. 1–9, 2020.
[23] C. F. Guimarães, L. Gasperini, A. P. Marques, and R. L. Reis, "The stiffness of living tissues and its implications for tissue engineering," *Nature Reviews Materials*, vol. 5, pp. 351–370, 2020.
[24] S. Vijayavenkataraman, L. Zhang, S. Zhang, J. Y. H. Fuh, and W. F. Lu, "Triply periodic minimal surfaces sheet scaffolds for tissue engineering applications: an optimization approach toward biomimetic scaffold design," *ACS Applied Bio Materials*, vol. 1, no. 2, pp. 259–269, 2018.
[25] N. S. Mustafa, N. H. Akhmal, S. Izman et al., "Application of computational method in designing a unit cell of bone tissue engineering scaffold: a review," *Polymers*, vol. 13, no. 10, Article ID 1584, 2021.
[26] Y. Jin, H. Kong, X. Zhou, G. Li, and J. Du, "Design and characterization of sheet-based gyroid porous structures with bioinspired functional gradients," *Materials*, vol. 13, no. 17, Article ID 3844, 2020.
[27] S. C. Han, J. M. Choi, G. Liu, and K. Kang, "A microscopic shell structure with Schwarz's D-surface," *Scientific Reports*, vol. 7, Article ID 13405, 2017.
[28] A. P. G. Castro, J. Santos, T. Pires, and P. R. Fernandes, "Micromechanical behavior of TPMS scaffolds for bone tissue engineering," *Macromolecular Materials and Engineering*, vol. 305, no. 12, Article ID 2000487, 2020.